Onslow, A. CE., Bogacz, R., & Jones, MW. (2011). Quantifying phase-amplitude coupling in neuronal network oscillations. *Progress in Biophysics and Molecular Biology*, *105*(1-2), 49-52. https://doi.org/10.1016/j.pbiomolbio.2010.09.007

Progress in Biophysics and Molecular Biology xxx (2010) 1–9

Contents lists available at ScienceDirect

Progress in Biophysics and Molecular Biology

journal homepage: www.elsevier.com/locate/pbiomolbio

Quantifying phase–amplitude coupling in neuronal network oscillations

Angela C.E. Onslow [a,b,c], Rafal Bogacz [b,**], Matthew W. Jones [c,*]

[a] Bristol Centre for Complexity Sciences, University of Bristol, UK
[b] Department of Computer Science, University of Bristol, UK
[c] School of Physiology & Pharmacology, University of Bristol, UK

ARTICLE INFO

Article history:
Available online xxx

Keywords:
Theta rhythm
Gamma rhythm
Hippocampus
Prefrontal cortex

ABSTRACT

Neuroscience time series data from a range of techniques and species reveal complex, non-linear interactions between different frequencies of neuronal network oscillations within and across brain regions. Here, we briefly review the evidence that these nested, cross-frequency interactions act in concert with linearly covariant (within-frequency) activity to dynamically coordinate functionally related neuronal ensembles during behaviour. Such studies depend upon reliable quantification of cross-frequency coordination, and we compare the properties of three techniques used to measure phase–amplitude coupling (PAC) – Envelope-to-Signal Correlation (ESC), the Modulation Index (MI) and Cross-Frequency Coherence (CFC) – by standardizing their filtering algorithms and systematically assessing their robustness to noise and signal amplitude using artificial signals. Importantly, we also introduce a freely-downloadable method for estimating statistical significance of PAC, a step overlooked in the majority of published studies. We find that varying data length and noise levels leads to the three measures differentially detecting false positives or correctly identifying frequency bands of interaction; these conditions should therefore be taken into careful consideration when selecting PAC analyses. Finally, we demonstrate the utility of the three measures in quantifying PAC in local field potential data simultaneously recorded from rat hippocampus and prefrontal cortex, revealing a novel finding of prefrontal cortical theta phase modulating hippocampal gamma power. Future adaptations that allow detection of time-variant PAC should prove essential in deciphering the roles of cross-frequency coupling in mediating or reflecting nervous system function.

Contents

* Corresponding author. School of Physiology & Pharmacology, Medical Sciences Building, University Walk, University of Bristol, Bristol BS8 1TD, UK. Tel.: +44 117 331 2289; fax: +44 117 331 2288.
** Corresponding author.
E-mail addresses: R.Bogacz@bristol.ac.uk (R. Bogacz), Matt.Jones@bristol.ac.uk (M.W. Jones).

0079-6107/$ – see front matter © 2010 Published by Elsevier Ltd.
doi:10.1016/j.pbiomolbio.2010.09.007

1. Introduction

Oscillatory activity is a pervasive feature of biological systems in general and nervous systems in particular. Neuronal oscillations reflect interdependencies between the relative timing (phase) and power (amplitude) of rhythmic activity in individual components of neurons, networks and systems. Oscillation cycle lengths range from milliseconds (e.g. 100–200 Hz hippocampal ripples), to seconds (e.g. cardio-respiratory rhythms in brainstem), to hours (e.g. circadian modulation of cortical excitability), with oscillations at these distinct frequencies arising from distinct cellular, synaptic and neuromodulatory processes (Buzsaki, 2006; Young and Eggermont, 2009). The powers of these diverse oscillatory frequencies can be dynamically modulated over a similar range of timescales, as can the coherence of a given frequency of oscillation between networks of neurons across numerous brain regions. This within-frequency coordination reflects and mediates functional connectivity, allowing specialized structures to both encode information independently and to interact selectively according to behavioural demands (Fries, 2009; Varela et al., 2001). However, rather than constituting independent communication channels analogous to AM radio signals, different frequencies of neuronal activity simultaneously interact with one another in nested, multiplexed signals. This cross-frequency coupling may reflect an important component of the synchronized neuronal activity believed to underlie brain function, and deciphering its mechanisms and roles necessitates increasingly sensitive and complex analyses and models.

1.1. Cross-frequency coupling in neuronal data

Cross-frequency coupling of neuronal activity is evident in at least two forms: (1) phase synchrony, during which a consistent number of higher-frequency cycles occur within single cycles of a lower-frequency rhythm (Tass et al., 1998) and (2) phase–amplitude coupling (PAC), during which the phase of a lower-frequency rhythm modulates the amplitude of a higher-frequency oscillation. Although the extent to which phase synchrony and PAC reflect similar mechanisms and roles remains to be established, both types of coupling are evident in a range of EEG, electrocorticogram (ECoG), magnetoencephalogram (MEG) and local field potential (LFP) data recorded from a range of brain regions and species. The majority of phase synchrony examples to date stem from studies of human neocortex (Darvas et al., 2009a,b; Palva et al., 2005; Palva and Palva, 2007); in contrast, PAC is prevalent in both human and rodent neocortical, allocortical and subcortical regions, and currently represents a more experimentally tractable model of cross-frequency coupling (see Jensen and Colgin, 2007).

The archetypal example of neuronal PAC was first uncovered in the CA1 subfield of the hippocampus, where LFP recordings reveal a consistent, cyclic variation of gamma-frequency (30–100 Hz) power with concurrent theta-frequency (5–10 Hz) phase (Bragin et al., 1995; see Fig. 1 for example). Since the connectivity and activity patterns of hippocampal excitatory and inhibitory principal neurons and interneurons are increasingly well understood (Klausberger and Somogyi, 2008), the hippocampus therefore

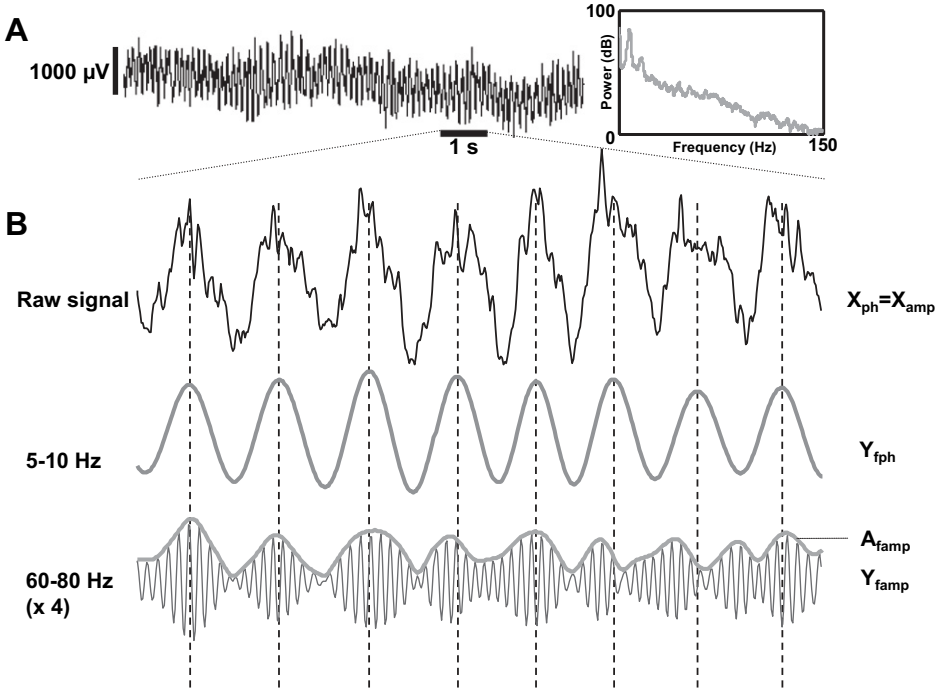

Fig. 1. Local field potential data showing theta–gamma PAC in CA1 of rat hippocampus. (A) 10 s of broadband LFP (left, bandpass filtered at 0.1–475 Hz) and corresponding power spectrum (right) showing predominant theta-frequency power whilst a rat actively explores its homecage. (B) Expanded 1 s segment showing raw signal (top) and bandpass filtered theta (middle, 5–10 Hz) and gamma (lower, 60–80 Hz, amplified by a factor of 4 for clarity) rhythms. The thick grey line over the gamma signal shows the amplitude envelope and dashed horizontal lines mark timing of theta cycle peaks; note alignment of theta peaks and gamma envelope during the first half of the trace. The notation to the right is defined in Methods and used throughout the text.

Please cite this article in press as: Onslow, A.C.E., et al., Quantifying phase–amplitude coupling in neuronal network oscillations, Progress in Biophysics and Molecular Biology (2010), doi:10.1016/j.pbiomolbio.2010.09.007

presents a valuable model network in which to dissect PAC's mechanisms and roles. For example, Wulff et al., 2009 used a genetically altered mouse line lacking functional GABA-A receptors on a subset of interneurons to suggest a role for rapid, synaptic feedback inhibition in shaping hippocampal PAC.

Models have attempted to link hippocampal theta–gamma PAC with CA1-dependent memory processing, whereby subsets of hippocampal units co-active during individual gamma cycles are recruited in consistent, sequential order dependent upon theta cycle phase (Lisman and Buzsaki, 2008; Lisman and Idiart, 1995; see also Fuentemilla et al., 2010). There is also evidence to suggest that hippocampal pyramidal cells differentiate in the preferred phase at which they fire in relation to theta–gamma PAC activity. This could allow for the simultaneous implementation of multiple coding schemes for memory items, stored in both a sequential and non-sequential context (Senior et al., 2008). Recent data from LFP recordings from both rat and human hippocampus provide evidence for a functional role of theta–gamma PAC in mnemonic processing (Axmacher et al., 2010; Shirvalkar et al., 2010; Tort et al., 2009), but these hippocampal models and examples also reflect a broader hypothesis of PAC function: hierarchies of inter-locked oscillatory frequencies allow ensembles of anatomically localized neurons co-active on short timescales (i.e. within higher-frequency cycles, e.g. Siegel et al., 2009) to be temporally aligned ('bound') across longer timescales and anatomical distances by lower-frequency modulation (see Sarnthein et al., 1998). VanRullen and Koch (2003) posited a PAC-based model of alpha–gamma-frequency interactions mediating perception, and a recent example of data supporting a functional role for hippocampal PAC showed that separable bands of the gamma-frequency range coincide with different phases of the theta rhythm in CA1. It was suggested that PAC of gamma at these different frequencies reflects the dynamic influence of afferent inputs from CA3 and entorhinal cortical regions to CA1 during different phases of the theta cycle (Colgin et al., 2009); as such, similar phenomena may reflect interactions in other systems of connected brain regions.

Beyond the hippocampal formation, PAC phenomena have been reported in sensory, frontal and parietal human neocortex during a range of auditory, linguistic and working memory tasks (Canolty et al., 2006; Osipova et al., 2008; Sauseng et al., 2008), plus in monkey auditory and visual cortices (Lakatos et al., 2007; Lakatos et al., 2008) and rodent olfactory bulb (see Rojas-Libano and Kay, 2008). The oscillation frequencies demonstrating PAC in these various systems and behaviours are by no means restricted to theta–gamma cross-frequency interactions, but also encompass delta (1–4 Hz) and alpha (8–12 Hz) rhythms, though variable definitions of frequency band labels can confound comparisons across species. Importantly, some studies suggest a continuous hierarchy of frequencies, with delta modulating theta which in turn modulates gamma (Lakatos et al., 2005); simultaneous PAC across such a range of timescales raises important questions about the underlying network structure giving rise to the phenomenon, as well as the relative functional contributions of oscillations at distinct frequencies.

Importantly, PAC does not occur only within functionally specialized brain regions, but also across functionally related brain regions. For example, hippocampal–striatal PAC is dynamically modulated alongside behavioural task demands in rat (Tort et al., 2008), and hippocampal theta phase can also modulate neocortical gamma power (Sirota et al., 2008). Like within-frequency coherence, PAC is therefore well placed to underpin or reflect the temporal coordination of neuronal networks across distributed brain regions, though the basic features of excitatory and inhibitory network connectivity that give rise to PAC of different frequencies and in different anatomical regions have not yet been established.

1.2. Analysis of phase–amplitude coupling

Fig. 1 shows 1 s of LFP data recorded from hippocampal CA1 of a freely behaving rat; whilst PAC is clearly evident upon visual inspection, these data demonstrate some central challenges that arise when attempting to quantify its extent and nature. These include, but are not limited to:

i. a variable signal-to-noise ratio between the amplitudes of both phase modulating and amplitude-modulated signal;
ii. estimating the statistical significance of any PAC present, given that PAC may arise by chance in signals simultaneously containing power in low and high frequencies;
iii. quantifying the time-variant dynamics of PAC, which is non-stationary and may come and go from one lower-frequency cycle to the next;
iv. limits imposed by the length of available data series, for example precluding analyses of low frequency signals;
v. establishing whether PAC applies to all frequencies present, or is restricted to specific pairs of modulating and modulated oscillations;
vi. determining whether amplitude-modulated power varies continuously with modulating phase, or whether step-like changes in amplitude underlie PAC.

Robust, sensitive analysis methods with sufficient temporal resolution and statistical power are therefore essential for the study of PAC, particularly in limited and/or noisy neurobiological data. A number of methods have been published in recent years, some of which have been compared and reviewed in different combinations elsewhere (Cohen, 2008; Penny et al., 2008; Tort et al., 2010). Here, we briefly review three of the available PAC analysis methods; we have standardized the algorithms for their implementation to enable an objective, quantifiable comparison of their advantages and limitations, which are demonstrated and discussed in relation to both simulated and real LFP data.

2. Methods

2.1. Notation

Throughout the following sections we denote the raw signals as $X_{ph}(t)$ and $X_{amp}(t)$, corresponding to the signal assumed to contain the lower, modulating frequency and the signal assumed to contain the higher, modulated frequency respectively. In analyses used to investigate the phase of a slower oscillation modulating the amplitude of a faster oscillation within the same signal, $X_{ph} = X_{amp}$. Each of the PAC detection measures relies on filtering one or both of these signals for particular frequencies. Y_{fph} will denote signal X_{ph} filtered for a particular frequency, *fph*. Y_{famp} will denote the signal X_{amp} filtered for a particular frequency, *famp*. Examples of the raw and filtered signals with corresponding notation can be seen in Fig. 1.

All the measures require the calculation of A_{famp}, the instantaneous amplitude envelope of the higher-frequency oscillation (also shown in Fig. 1). The MI measure also requires the instantaneous phase of the lower-frequency oscillation, denoted $\theta_{fph}(t)$. These are calculated by first obtaining an analytic representation of the appropriate signal, either using the Hilbert transform or filtering the signal via convolution with complex Morlet wavelets. The instantaneous amplitude and phase can then be calculated as the absolute value and the phase angle of the analytic signal respectively.

Please cite this article in press as: Onslow, A.C.E., et al., Quantifying phase–amplitude coupling in neuronal network oscillations, Progress in Biophysics and Molecular Biology (2010), doi:10.1016/j.pbiomolbio.2010.09.007

2.2. The Envelope-to-Signal (ESC) measure (Bruns and Eckhorn, 2004)

The ESC measure calculates the correlation between the amplitude envelope of the filtered high frequency signal, A_{famp}, and the filtered low frequency signal, Y_{fph}.

$$\mathrm{ESC}_{fph,\,famp} = r\left(A_{famp}, Y_{fph}\right)$$

2.3. The Modulation Index (MI) (Canolty et al., 2006)

The MI measure generates a complex valued composite signal such that the amplitude is composed of the high frequency amplitude envelope values, A_{famp}, and the phase is composed of the low frequency signal's instantaneous phase, $\theta_{fph}(t)$.

$$Z_{fph,\,famp}(t) = A_{famp}(t)\cdot e^{i\theta_{fph}(t)}$$

This composite signal creates a joint probability density function when viewed on the complex plane. If the average of the signal is non-zero then, assuming the distribution of *fph* phase values is uniform, this indicates a tendency for a particular amplitude and phase value to co-occur in time. An MI value is calculated as the absolute value of the average of the composite signal:

$$\mathrm{MI}_{fph,\,famp} = \left|\mathrm{average}\left(Z_{fph,famp}(t)\right)\right|$$

2.4. Cross-Frequency Coherence (CFC) (Osipova et al., 2008)

The CFC measure calculates the coherence at frequency *fph* between two signals: the time-varying energy of the high frequency signal (calculated as A_{famp} divided by half the sampling frequency and then squared, denoted $\tilde{A}_{famp}$) and the unfiltered raw signal believed to contain the modulating frequency, X_{ph}.

$$\mathrm{CFC}_{fph,\,famp} = \mathrm{coherence}_{fph}\left(X_{ph}, \tilde{A}_{famp}\right)$$

2.5. Standardization and implementation

The three PAC detection measures were implemented in a MATLAB toolbox, available at http://www.cs.bris.ac.uk/Research/MachineLearning/pac/

In order to directly compare the measures, a common method of filtering the data was employed. We chose to filter via convolution with complex Morlet wavelets with width = 7. Preliminary tests with various different types of filters showed that an acceptable alternative to wavelet filtering is to use a two-way least squares filter such as that implemented by the *eegfilt* function (part of the EEGLAB toolbox for MATLAB http://sccn.ucsd.edu/eeglab/). Infinite Impulse Response filters such as the Butterworth filter do not have sufficient frequency response characteristics to capture the necessary time-frequency information which determines PAC signals.

Our implementation of the three measures also includes a method of statistical significance testing; again this is common to all three measures. The high frequency amplitude envelope signal is shuffled in order to disrupt the time-ordering of values. This is achieved by dividing the data into sections, the number of which is set equal to the number of seconds of data or 1000, whichever is the larger value. The boundaries of the sections are placed at random locations chosen with uniform probability throughout the signal. The sections are then rearranged at random to create the final shuffled signal. This procedure retains the mean, variance and power spectrum of the original signal whilst removing the temporal relationship between amplitude values. Discontinuities are introduced and there is evidence that this can introduce spurious PAC detection results (Kramer et al., 2008), however the performance on artificial data was still deemed sufficient, presumably since the discontinuities are independently distributed in time. A population of 50 shuffled signals are created and compared to the original low frequency signal in order to generate a distribution of PAC values using the appropriate measure. PAC values lying in the top 5% of this distribution were deemed significant.

2.6. Generation of artificial data

In order to test the performance of the three PAC detection measures we generated artificial data in which we could control if and to what extent PAC occurs. Since the majority of neuronal recordings presenting PAC focus on theta modulating gamma rhythms (Bragin et al., 1995) we chose to create signals containing power at *fph* = 4 Hz and *famp* = 60 Hz. The sampling frequency *Fs* = 1017 Hz.

To build our data first we generated two signals, one oscillating at *fph* and one at *famp*:

$$\mathrm{sig}_{fph}(t) = \sin((fph/Fs)2\pi t) \tag{2.4.1}$$

$$\mathrm{sig}_{famp}(t) = \sin((famp/Fs)2\pi t) \tag{2.4.2}$$

Artificial data without PAC were generated by simply adding these two signals and some Gaussian white noise, *WN*:

$$\mathrm{sig}_{noPAC} = \mathrm{sig}_{fph}(t) + \mathrm{sig}_{famp}(t) + \sigma\cdot WN \tag{2.4.3}$$

where σ is the standard deviation of *WN*, used as a scaling factor to increase the level of noise.

Artificial data containing PAC were generated in a similar way to amplitude-modulated radio waves, forming the product of $\mathrm{sig}_{famp}(t)$ and the signal $\mathrm{sig}_{fph}(t)$ increased by 1 (so its minimum is at 0), and adding white noise:

$$X_{amp}(t) = K\cdot\mathrm{sig}_{famp}(t)\cdot\left(\mathrm{sig}_{fph}(t)+1\right) + \sigma\cdot WN \tag{2.4.4}$$

where K = a scaling factor used to control the amplitude of the 60Hz signal.

A second artificial signal, $X_{ph}(t)$, containing only an oscillation at *fph* = 4 Hz and some white noise was used as a comparison signal.

$$X_{ph}(t) = \mathrm{sig}_{fph}(t) + \sigma\cdot WN \tag{2.4.5}$$

Sample artificial signals are shown in Fig. 2A. It is possible to add this component signal to the signal containing PAC, $X_{amp}(t)$, and then compare this signal with itself in order to look for coupled frequencies, however this has a tendency to produce spurious artifacts with some of the measures.

2.7. Quantifying the performance of PAC measures

Several related tests were conducted to compare the performance of ESC, MI and CFC methods.

2.7.1. False positives

In order to test whether the measures would erroneously report significant PAC when it was not engineered into artificial data, we generated 10 s of $X_{noPAC}(t)$, (see Equation 2.4.3). The PAC detection measures were tested by comparing this signal with itself and looking for false coupling at 4 Hz modulating 60 Hz. This test was repeated for 1000 iterations for each measure.

Please cite this article in press as: Onslow, A.C.E., et al., Quantifying phase–amplitude coupling in neuronal network oscillations, Progress in Biophysics and Molecular Biology (2010), doi:10.1016/j.pbiomolbio.2010.09.007

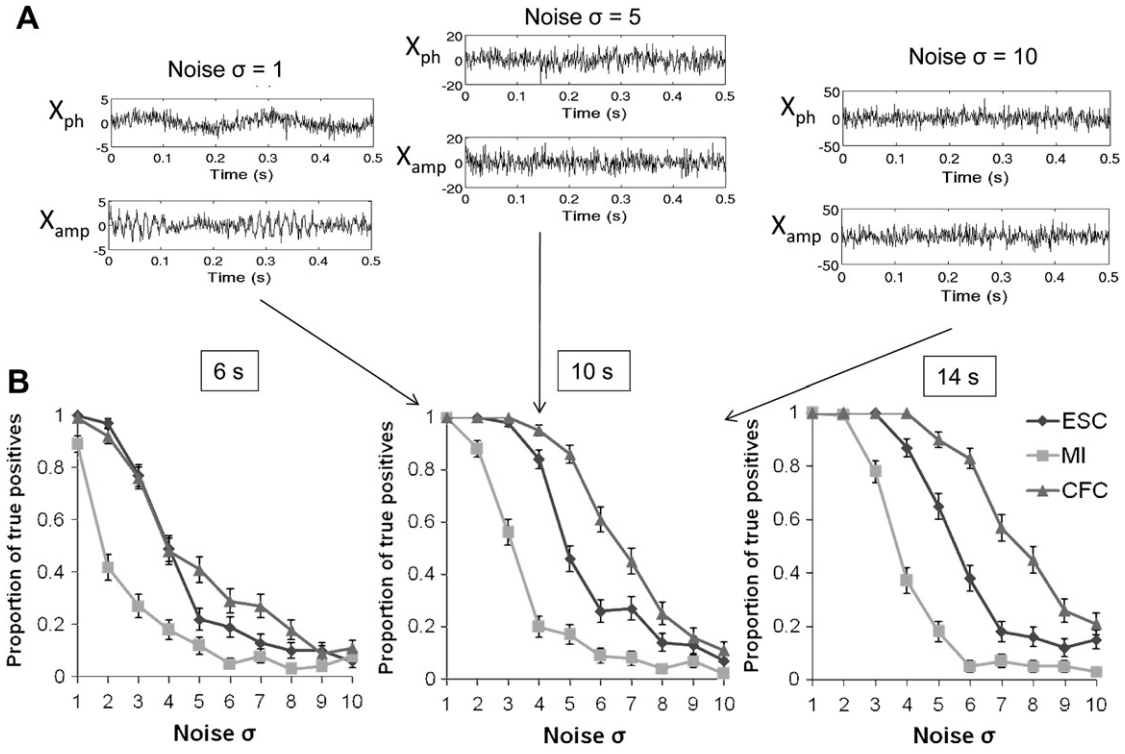

Fig. 2. Comparison of true positive detection as a function of varying noise level and data length. (A) Raw simulated data signals containing 4 Hz modulating 60 Hz PAC, generated with different noise levels. Examples show standard deviation, σ, of white noise set to 1, 5 and 10 respectively; arrows point to corresponding points on analysis graph. (B) Mean proportions of true positives (defined as significant PAC located within $f_{ph} = 1$–15 Hz and $f_{amp} = 45$–75 Hz) detected by each of the three PAC measures with increasing noise levels (dark grey diamonds ESC; light grey squares MI; mid grey triangles CFC). Left to right panels show the same experiment conducted on 6 s, 10 s and 14 s signals. Error bars show ±s.e.m.

2.7.2. True positives and data length-dependence

The PAC detection measures were tested by comparing the PAC containing signal, $X_{amp}(t)$ (Equation 2.2.4), with the signal containing the modulating frequency, $X_{ph}(t)$ (Equation 2.2.5), and looking for coupling at 4 Hz modulating 60 Hz. This test was repeated for 100 iterations. The standard deviation of the noise was increased to see how this affected the true positive detection rate. These experiments were repeated with artificial signals of length 6, 10 and 14 s, in order to examine data length-dependence.

2.7.3. Correct detection of PAC frequencies as a function of increasing noise

We then tested to see if the highest value of PAC detected by each of the measures occurs at frequencies close to the true *fph* and *famp* contained in the artificial data. As for the true positive tests previously, the standard deviation of the noise was increased and at each level the three PAC measures were tested, comparing the PAC containing signal, $X_{amp}(t)$, with the signal containing the modulating frequency, $X_{ph}(t)$. In these tests however, the measures were employed to look for PAC over a range of possible frequencies: from 1 Hz to 101 Hz in bands of 5 Hz width. The first frequency bin of interest (in terms of both *fph* and *famp*) was from 1 to 5 Hz, with the centre frequency defining the appropriate wavelet kernel set at 3 Hz, the second was from 6 to 10 Hz, with the centre frequency set at 8 Hz and so on. Investigation of a range of possible coupling frequency values allowed the creation of a 'PACgram', highlighting the frequencies between which the strongest coupling was found using a colour scale. A correct detection was defined as the largest PAC value occurring in a region of sufficient frequency resolution surrounding the correct value of 4 modulating 60 Hz. This region was determined to be between 1 and 15 Hz in terms of the modulating frequency, *fph*, and between 45 and 75 Hz in terms of the modulated frequency, *famp*, allowing up to 10 Hz margin for error along the *x*-axis of the PACgram and up to 15 Hz along the *y*-axis.

2.7.4. Correct detection of PAC frequencies as a function of decreasing amplitude envelope magnitude

We then investigated the performance of the measures as the amplitude of the higher-frequency oscillation decreases. The experiments described in Section 2.5.3 were modified, the noise level of the generated signals, $X_{ph}(t)$ and $X_{amp}(t)$, was kept constant at $\sigma = 1$ and instead the amplitude of the 60 Hz oscillation ($\text{sig}_{amp}(t)$) was decreased by a scaling factor K. Again the signals were examined between 1 and 101 Hz in bands of 5 Hz in order to create PACgrams and the same criteria for correct detection was applied.

3. Results and discussion

We first tested if the methods detect statistically significant PAC at a fixed combination of frequencies (4 Hz modulating 60 Hz was used throughout simulations, modeling the theta–gamma PAC reported in a range of neural data) in artificial data that did not contain PAC. As we expected all methods detected significant PAC on average on 5% of simulated signals, and there were no statistically significant differences between the methods.

Unsurprisingly, consistent detection of statistically significant PAC in artificially-generated signals containing PAC was dependent upon noise levels and data length. As shown in Fig. 2, MI, ESC and CFC methods all correctly identified significant PAC at the fixed combination of frequencies under low noise conditions; with high

noise, the statistical properties of our shuffling procedure gave rise to mistaken PAC detection on approximately 5% of trials, satisfying the preset false positive rate of alpha = 0.05. CFC consistently outperformed ESC and MI across intermediate noise levels, with CFC's advantage becoming more apparent as the length of data analysed was increased from 6 s to 14 s (Fig. 2B). Improvements in the performance of MI and CFC with data length are also shown for real data in Fig. 4, and are a consistent feature of these analyses. Nevertheless, these simulations demonstrate that CFC may be the better choice of analysis method for short duration, noisy signals, particularly given *a priori* reasons to examine PAC at a specific combination of f_{ph} and f_{amp} frequencies.

The analysis in Fig. 2 focused on a single PAC frequency pairing of 4 Hz and 60 Hz signals, thereby ignoring any erroneous PAC detection at other frequencies. In contrast, Fig. 3 quantifies the proportion of significant PAC detected within the appropriate frequency ranges (1–15 Hz modulating 45–75 Hz) in the face of increasing noise; erroneous detection of significant PAC elsewhere in the frequency spectrum can therefore contribute to poor performance by this measure. MI, ESC and CFC methods performed similarly in this test. CFC was slightly more consistent at intermediate noise levels, but dropped to lower performance than MI and ESC at high noise. The low proportion of correctly identified PAC by CFC at high noise levels shown in Fig. 3 is due to incorrectly detected regions of PAC at frequencies outside the ranges specified as correct (see also example in Fig. 5A). MI appears able to detect significant PAC in the correct frequency region even on approximately 40% of high noise trials, though did generate some variability in precise PAC frequencies detected. This remarkable robustness to noise is not purely artefactual, since MI only detects significant PAC in the expected 5% of tests on independent signals. Further tests are therefore required to establish whether this reflects a tendency of MI to detect significant PAC at low f_{ph} frequencies.

The analyses shown in Fig. 4, like those in Fig. 3, are based upon correct detection of PAC in appropriate frequency ranges (again with 4 Hz modulating 60 Hz in the simulated data), but with varying $X_{amp}(t)$ 60 Hz power rather than varying noise levels in $X_{amp}(t)$. Accuracy of ESC and MI measures was consistently higher than of CFC until 60 Hz amplitude was scaled by a factor $\mathbf{K} \geq 0.02$; all three measures performed optimally given higher 60 Hz power.

Fig. 5 demonstrates the performance of ESC, MI and CFC techniques on real LFP data recorded simultaneously from hippocampal CA1 and deep layers of the medial prefrontal cortex (mPFC; prelimbic subdivision) using chronically implanted, microwire electrodes in an adult male, Lister Hooded rat freely behaving in a familiar homecage (see Jones and Wilson, 2005 for recording details). Fig. 5A shows that all methods detected statistically

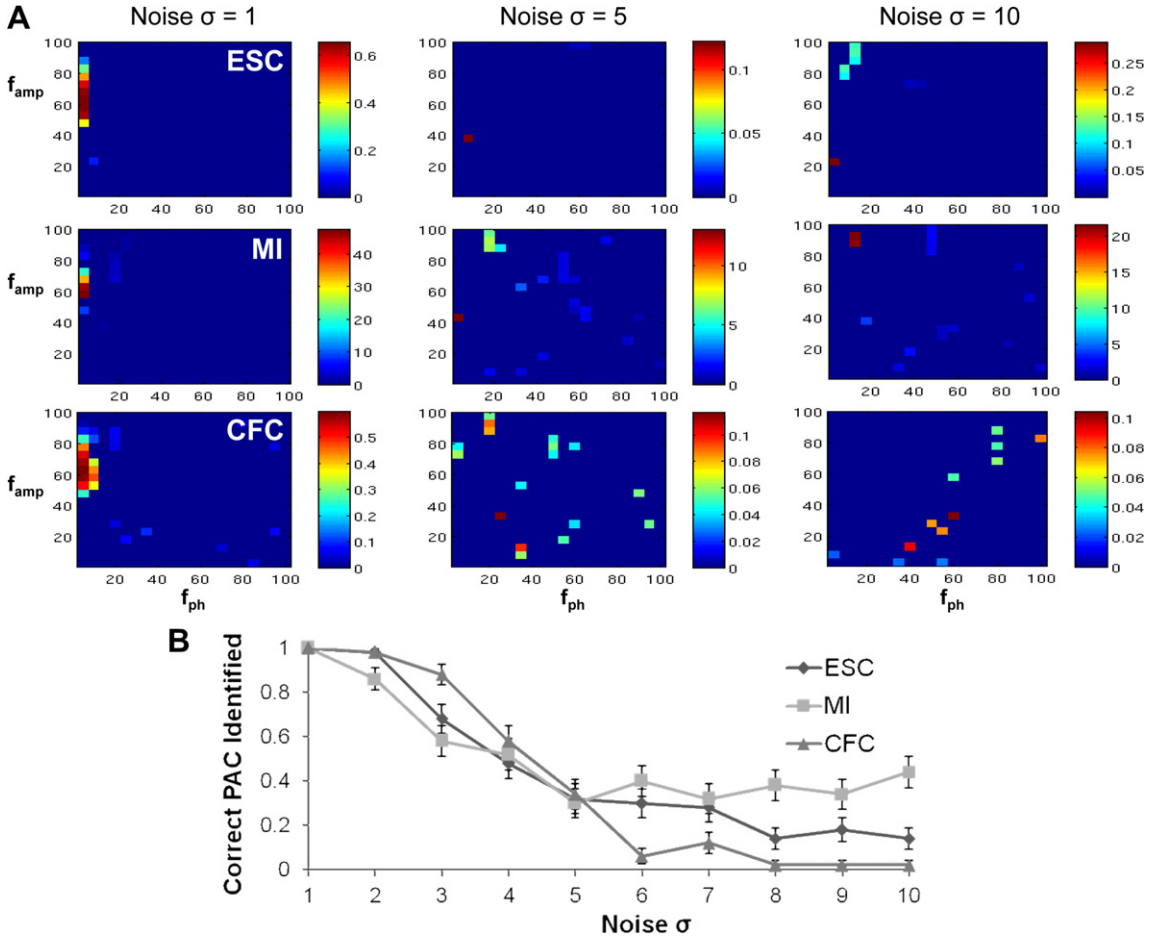

Fig. 3. Correct identification of PAC as a function of signal noise level. 10 s simulated signals containing 4 Hz modulating 60 Hz PAC were created and the standard deviation of the noise added was increased. Performance was scored by quantifying the proportion of trials in which maximal PAC was correctly located within f_{ph} = 1–15 Hz and f_{amp} = 45–75 Hz. (A) Example PACgrams generated by ESC, MI and CFC measures as standard deviation of the noise, σ, varied from 1, 5 and 10. Colour scale represents the magnitude of PAC found. Pixels in which no significant PAC was detected are set to 0. Note different colour scales. (B) Mean results showing decreasing performance as noise levels increase (dark grey diamonds ESC; light grey squares MI; mid grey triangles CFC). Error bars show ±s.e.m.

Please cite this article in press as: Onslow, A.C.E., et al., Quantifying phase–amplitude coupling in neuronal network oscillations, Progress in Biophysics and Molecular Biology (2010), doi:10.1016/j.pbiomolbio.2010.09.007

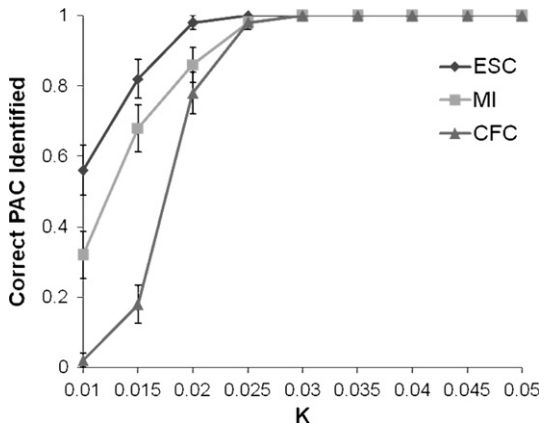

Fig. 4. Correct identification of PAC as a function of gamma envelope amplitude. Simulated signals containing 4 Hz modulating 60 Hz PAC were created (10 s, standard deviation of noise = 1) with decreasing 60 Hz signal amplitudes. The horizontal axis shows the scaling factor K used to control the amplitude of the 60 Hz signal (see Equation 2.4.4). ESC, MI and CFC performance was tested by quantifying the highest level of PAC in the region of $f_{ph} = 1$–15 Hz and $f_{amp} = 45$–75 Hz. Mean ± s.e.m. is shown for values of **K** between 0.01 and 0.05.

significant intra-hippocampal PAC consistent with previous reports, with 5–10 Hz theta phase modulating power of gamma oscillations at 60–80 Hz. None of the methods detected significant intra-cortical PAC (data not shown). However, important differences between methods became apparent when analyses are applied to 6 s *vs.* 1 min data segments. Whilst all three methods detected theta–gamma coupling at the expected frequencies during the 6 s data segment, ESC reported PAC in a much more restricted frequency range than MI and CFC, with the latter in particular detecting some significant PAC at higher frequencies. Of course, lower right-hand regions of the PAC plots reflect impossible combinations of higher frequencies modulating lower frequencies and can be ignored. Nevertheless, the extent to which all statistically significant PAC detected by CFC reflects real neurophysiological processes remains to be established.

Analysis of a continuous, 1 min data segment tends to focus MI and CFC PAC estimates, though CFC still reports significant PAC at higher frequencies; in contrast, the theta–gamma PAC magnitude estimated by ESC reduces in comparison to the 6 s analysis. The most likely cause of variance between 6 s and 1 min estimates is non-stationary PAC during the longer segment, which has differential impact on the methods used here. The ESC measure is more sensitive to intermittent PAC, since non-coupled epochs within a longer segment will decrease the value of the overall correlation

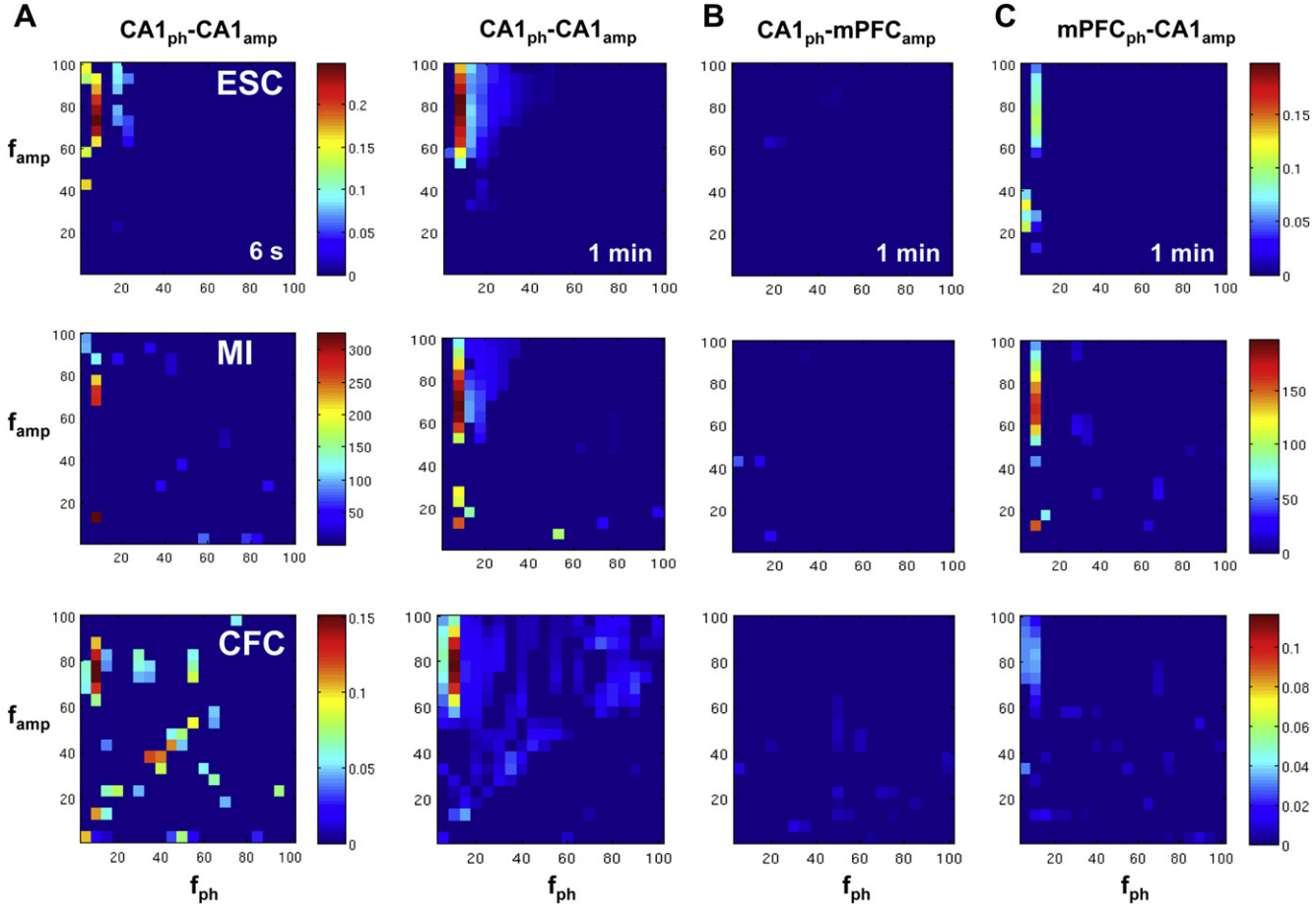

Fig. 5. Detection of PAC in local field potentials recorded simultaneously from rat hippocampus and prefrontal cortex. (A) ESC (top row), MI (middle row) and CFC (lower row) analyses of 6 s (left column) and 1 min (right column) of continuous LFP recorded from CA1 of rat hippocampus, demonstrating theta–gamma PAC consistent with previous reports. (B) Cross-structural PAC analysis of simultaneously recorded CA1 and mPFC LFP, showing lack of robust modulation of mPFC gamma power by CA1 theta phase during this 1 min recording segment. (C) In contrast to (B), mPFC theta phase does modulate CA1 gamma power in these data. Colour scales vary from 6 s to 1 min analyses, but are consistent for each of the three methods for $CA1_{ph}$–$CA1_{amp}$, $CA1_{ph}$–$mPFC_{amp}$ and $mPFC_{ph}$–$CA1_{amp}$ panels. Pixels in which no significant PAC was detected are set to 0.

Please cite this article in press as: Onslow, A.C.E., et al., Quantifying phase–amplitude coupling in neuronal network oscillations, Progress in Biophysics and Molecular Biology (2010), doi:10.1016/j.pbiomolbio.2010.09.007

between lower-frequency phase and higher-frequency amplitude envelope. Therefore reduced ESC magnitude in Fig. 5A (note different colour scales) presumably reflects non-correlated (or noisy/lower power) theta–gamma epochs within the 1 min segment. With the MI measure, even intermittent coupling cumulatively contributes to greater magnitudes of PAC at a particular combination of frequencies; unless modulating and modulated frequencies change and signals fall into another coupling relationship for a sustained amount of time, PAC magnitude at a given combination of frequencies will be proportional to the length of data analysed. Similarly, the coherence estimates employed by CFC are averaged over sliding windows, hence non-stationary coupling does not necessarily degrade overall PAC estimates. Note that unlike ESC and CFC, MI detects a region of lower-frequency PAC in the 1 min segment analysed here. Again, this may reflect a weighting of MI towards low frequency combinations.

Fig. 5A therefore demonstrates that MI or CFC methods can prove superior when analyses are required to quantify averaged PAC levels over sustained recording periods. However, such averaging of course masks underlying PAC dynamics, which are certainly of interest when correlating PAC changes with other neurophysiological parameters and/or behaviour. ESC, MI and CFC measures can all be adapted (within the constraints of the methods' frequency resolutions) to allow characterization of time-variant PAC using a windowing approach. These adaptations are likely to prove critical to further elucidating PAC mechanisms and functions.

Fig. 5B shows analysis of cross-structural, CA1–mPFC PAC. Previous studies using similar recording techniques have reported that the phase of hippocampal theta modulates the power of neocortical gamma in rodents (Adhikari et al., 2010; Sirota et al., 2008). Indeed, the directionality of this reported CA1–mPFC PAC fits intuitively with known anatomical and functional connectivity in this limbic-cortical system since (i) the hippocampal formation sends direct, excitatory projections to mPFC (see Thierry et al., 2000) whereas direct, reciprocal projections from mPFC to CA1 have not been described and (ii) the relative timing of mPFC neuron action potentials phase-locked to CA1 theta oscillations is consistent with CA1 activity leading mPFC activity in this frequency range (Siapas et al., 2005). Hippocampal projections to mPFC are therefore well placed to control timing of mPFC networks. However, none of the three methods used here detected robust CA1–mPFC PAC in these sample data. Differences between these reports are likely to reflect differences in behavioural state since – like CA1–mPFC theta-frequency coherence (Jones and Wilson, 2005) – the extent of CA1–mPFC PAC is presumably highly dependent upon ongoing behaviour in general, and cognitive behaviours recruiting CA1–mPFC interactions in particular.

Fig. 5C shows the first reported example – to our knowledge – of mPFC theta phase modulating the power of CA1 gamma oscillations. This mPFC–CA1 PAC occurs at very similar frequencies to those simultaneously detected within the hippocampus (Fig. 4A), though is lower in magnitude and not associated with the higher modulating-frequency PAC detected in CA1, raising the possibility that the higher *fph* PAC evident in Fig. 5A may only be detected in local, intra-network analyses. Further experiments are required to rule out volume conduction artefacts in these LFP data (see Sirota et al., 2008), and further analyses of PAC dynamics are required to relate the timing of mPFC–CA1 PAC to CA1–CA1 and CA1–mPFC coupling. Given the lack of direct projections from mPFC to CA1, coupling in this direction presumably reflects indirect, polysynaptic influence of mPFC on CA1, potentially via entorhinal cortex. Nevertheless, the detection of mPFC–CA1 PAC raises the possibility that bi-directional, theta–gamma cross-frequency coupling is dissociable from theta-frequency coherence and reflects additional mechanisms of interaction between hippocampus and mPFC.

4. Conclusions

We present adaptations to ESC, MI and CFC methods that allow estimates of statistical significance of PAC, thus addressing important concerns that the phenomenon may reflect passive spectral properties of mixed-frequency signals, rather than underlying neurophysiology. These statistical methods are critical in consistently quantifying PAC levels, particularly when comparing different experimental, physiological and pathological conditions. For example, quantifying the impact of pharmacological and genetic manipulations on PAC is likely to provide critical insight into mechanisms (Wulff et al., 2009), and quantifying abnormal PAC in disease states may reveal roles in generating complex, information processing impairments in neuro-psychiatric disorders (Jones, 2010; Lisman and Buzsaki, 2008).

Though ESC, MI and CFC measures are all derived from similar fundamental principles, analyses of simulated data did reveal dissociable sensitivity and accuracy during varying conditions of noise, signal amplitude and data length. No one measure unfailingly out-performed the others: CFC is well-suited to applications with short data series in which known combinations of frequencies are coupled (Fig. 2), but gives less reliable results than MI or ESC when surveying noisy data for unknown frequency regions of coupling (Fig. 3), or when f_{amp} power is low (Fig. 4). Whilst MI and CFC methods are better-suited than ESC to quantification of overall mean PAC strength in extended time series, the adaptation of all methods to allow assessment of time-variant PAC should negate ESC's shortcomings in this regard. These adaptations will constitute an essential step towards relating PAC and behavioural dynamics.

All three of the measures implemented here are relatively computationally intensive in their own right, and more so when combined with the shuffling procedure used to estimate statistical significance. Practical constraints are therefore worthy of consideration, particularly when faced with large volumes of continuous data. ESC and MI algorithms consistently ran more quickly than CFC, though this issue may be partially bypassed if experimental design allows for analysis of relatively brief <10 s sections or trials of data.

Future work could improve the computational efficiency by only generating PACgram values for frequency combinations falling in the top half of the matrix, above the main diagonal (bottom left to top right), since frequency combinations below cannot represent valid PAC by our definition. This was not done during the current analyses in order to ascertain if any of the measures suffered from serious problems with artifactual PAC detection at any given combination of frequencies. In addition, there may be computational benefits to using a Fourier transform based phase randomization procedure (Theiler et al., 1992) to produce surrogate data; this may also improve detection accuracy by removing the discontinuities which the current procedure introduces which can generate spurious high frequency signal components. An interesting extension would be to compare the performance of the measures on synthetic data generated from computational models.

Whilst theta–gamma PAC within the hippocampus is increasingly well understood in terms of mechanism and function, recent reports of PAC across other, related brain systems implicate cross-frequency coupling more broadly in coordinating neuronal network function, particularly in relation to complex, cognitive behaviours. Future work establishing the structure of basic network motifs enabling PAC should therefore extend understanding of its mechanisms and roles; these certainly reach beyond theta–gamma oscillation timescales, and may reach beyond limbic-cortical neuronal networks to other circuits featuring rhythmic activity. For example, it became apparent during the 'Brain Modes' workshop highlighted in this issue that PAC-like phenomena also arise in

Please cite this article in press as: Onslow, A.C.E., et al., Quantifying phase–amplitude coupling in neuronal network oscillations, Progress in Biophysics and Molecular Biology (2010), doi:10.1016/j.pbiomolbio.2010.09.007

pulsatile hormone secretions (Walker et al., 2010). Cross-frequency coupling may therefore arise in a number of biological systems built upon delayed feedback, reflecting a universal role in coordinating rhythmic activity across varied timescales.

Acknowledgements

Our thanks to Ole Jensen of the F.C. Donders Centre for Cognitive Neuroimaging for generous sharing of CFC Matlab code. Related tools are freely available at: http://megcommunity.org/index.php?option=com_content&view=article&id=30&Itemid=36.

LFP data were kindly provided by Hannah Chandler (University of Bristol, Department of Physiology and Pharmacology); MWJ thanks the MRC, BBSRC and The Wellcome Trust for financial support of related experimental work. ACEO is supported by the EPSRC grant EP/E501214/1.

References

Adhikari, A., Topiwala, M.A., Gordon, J.A., 2010. Synchronized activity between the ventral hippocampus and the medial prefrontal cortex during anxiety. Neuron 65, 257–269.

Axmacher, N., Henseler, M.M., Jensen, O., Weinreich, I., Elger, C.E., Fell, J., 2010. Cross-frequency coupling supports multi-item working memory in the human hippocampus. Proc. Natl. Acad. Sci. U.S.A. 107, 3228–3233.

Bragin, A., Jando, G., Nadasdy, Z., Hetke, J., Wise, K., Buzsaki, G., 1995. Gamma (40–100 Hz) oscillation in the hippocampus of the behaving rat. J. Neurosci. 15, 47–60.

Bruns, A., Eckhorn, R., 2004. Task-related coupling from high- to low-frequency signals among visual cortical areas in human subdural recordings. Int. J. Psychophysiol. 51, 97–116.

Buzsaki, G., 2006. Rhythms of the Brain. Oxford University Press, Inc., Oxford.

Canolty, R.T., Edwards, E., Dalal, S.S., Soltani, M., Nagarajan, S.S., Kirsch, H.E., Berger, M.S., Barbaro, N.M., Knight, R.T., 2006. High gamma power is phase-locked to theta oscillations in human neocortex. Science 313, 1626–1628.

Cohen, M.X., 2008. Assessing transient cross-frequency coupling in EEG data. J. Neurosci. Methods 168, 494–499.

Colgin, L.L., Denninger, T., Fyhn, M., Hafting, T., Bonnevie, T., Jensen, O., Moser, M.B., Moser, E.I., 2009. Frequency of gamma oscillations routes flow of information in the hippocampus. Nature 462, 353–357.

Darvas, F., Miller, K.J., Rao, R.P., Ojemann, J.G., 2009a. Nonlinear phase–phase cross-frequency coupling mediates communication between distant sites in human neocortex. J. Neurosci. 29, 426–435.

Darvas, F., Ojemann, J.G., Sorensen, L.B., 2009b. Bi-phase locking – a tool for probing non-linear interaction in the human brain. Neuroimage 46, 123–132.

Fries, P., 2009. Neuronal gamma-band synchronization as a fundamental process in cortical computation. Annu. Rev. Neurosci. 32, 209–224.

Fuentemilla, L., Penny, W.D., Cashdollar, N., Bunzeck, N., Duzel, E., 2010. Theta-coupled periodic replay in working memory. Curr. Biol. 20, 606–612.

Jensen, O., Colgin, L.L., 2007. Cross-frequency coupling between neuronal oscillations. Trends Cogn. Sci. 11, 267–269.

Jones, M.W., 2010. Errant ensembles: dysfunctional neuronal network dynamics in schizophrenia. Biochem. Soc. Trans. 38, 516–521.

Jones, M.W., Wilson, M.A., 2005. Theta rhythms coordinate hippocampal–prefrontal interactions in a spatial memory task. PLoS Biol. 3, e402.

Klausberger, T., Somogyi, P., 2008. Neuronal diversity and temporal dynamics: the unity of hippocampal circuit operations. Science 321, 53–57.

Kramer, M.A., Tort, A.B., Kopell, N.J., 2008. Sharp edge artifacts and spurious coupling in EEG frequency comodulation measures. J. Neurosci. Methods 170, 352–357.

Lakatos, P., Chen, C.M., O'Connell, M.N., Mills, A., Schroeder, C.E., 2007. Neuronal oscillations and multisensory interaction in primary auditory cortex. Neuron 53, 279–292.

Lakatos, P., Karmos, G., Mehta, A.D., Ulbert, I., Schroeder, C.E., 2008. Entrainment of neuronal oscillations as a mechanism of attentional selection. Science 320, 110–113.

Lakatos, P., Shah, A.S., Knuth, K.H., Ulbert, I., Karmos, G., Schroeder, C.E., 2005. An oscillatory hierarchy controlling neuronal excitability and stimulus processing in the auditory cortex. J. Neurophysiol. 94, 1904–1911.

Lisman, J., Buzsaki, G., 2008. A neural coding scheme formed by the combined function of gamma and theta oscillations. Schizophr. Bull. 34, 974–980.

Lisman, J.E., Idiart, M.A., 1995. Storage of 7 +/− 2 short-term memories in oscillatory subcycles. Science 267, 1512–1515.

Osipova, D., Hermes, D., Jensen, O., 2008. Gamma power is phase-locked to posterior alpha activity. PLoS One 3, e3990.

Palva, J.M., Palva, S., Kaila, K., 2005. Phase synchrony among neuronal oscillations in the human cortex. J. Neurosci. 25, 3962–3972.

Palva, S., Palva, J.M., 2007. New vistas for alpha-frequency band oscillations. Trends Neurosci. 30, 150–158.

Penny, W.D., Duzel, E., Miller, K.J., Ojemann, J.G., 2008. Testing for nested oscillation. J. Neurosci. Methods 174, 50–61.

Rojas-Libano, D., Kay, L.M., 2008. Olfactory system gamma oscillations: the physiological dissection of a cognitive neural system. Cogn. Neurodyn. 2, 179–194.

Sarnthein, J., Petsche, H., Rappelsberger, P., Shaw, G.L., von Stein, A., 1998. Synchronization between prefrontal and posterior association cortex during human working memory. Proc. Natl. Acad. Sci. U.S.A. 95, 7092–7096.

Sauseng, P., Klimesch, W., Gruber, W.R., Birbaumer, N., 2008. Cross-frequency phase synchronization: a brain mechanism of memory matching and attention. Neuroimage 40, 308–317.

Senior, T.J., Huxter, J.R., Allen, K., O'Neill, J., Csicsvari, J., 2008. Gamma oscillatory firing reveals distinct populations of pyramidal cells in the CA1 region of the hippocampus. J. Neurosci. 28, 2274–2286.

Shirvalkar, P.R., Rapp, P.R., Shapiro, M.L., 2010. Bidirectional changes to hippocampal theta–gamma comodulation predict memory for recent spatial episodes. Proc. Natl. Acad. Sci. U.S.A. 107, 7054–7059.

Siapas, A.G., Lubenov, E.V., Wilson, M.A., 2005. Prefrontal phase locking to hippocampal theta oscillations. Neuron 46, 141–151.

Siegel, M., Warden, M.R., Miller, E.K., 2009. Phase-dependent neuronal coding of objects in short-term memory. Proc. Natl. Acad. Sci. U.S.A. 106, 21341–21346.

Sirota, A., Montgomery, S., Fujisawa, S., Isomura, Y., Zugaro, M., Buzsaki, G., 2008. Entrainment of neocortical neurons and gamma oscillations by the hippocampal theta rhythm. Neuron 60, 683–697.

Tass, P., Rosenblum, M.G., Weule, J., Kurths, J., Pikovsky, A., Volkmann, J., Schnitzler, A., Freund, H.J., 1998. Detection of n:m phase locking from noisy data: application to magnetoencephalography. Phys. Rev. Lett. 81, 3291–3294.

Theiler, J., Eubank, S., Longtin, A., Galdrikian, B., Farmer, J.D., 1992. Testing for nonlinearity in time series: the method of surrogate data. Phys. D 58, 77–94.

Thierry, A.M., Gioanni, Y., Degenetais, E., Glowinski, J., 2000. Hippocampo-prefrontal cortex pathway: anatomical and electrophysiological characteristics. Hippocampus 10, 411–419.

Tort, A.B., Komorowski, R., Eichenbaum, H., Kopell, N.J., 2010. Measuring phase–amplitude coupling between neuronal oscillations of different frequencies. J. Neurophysiol..

Tort, A.B., Komorowski, R.W., Manns, J.R., Kopell, N.J., Eichenbaum, H., 2009. Theta–gamma coupling increases during the learning of item-context associations. Proc. Natl. Acad. Sci. U.S.A..

Tort, A.B., Kramer, M.A., Thorn, C., Gibson, D.J., Kubota, Y., Graybiel, A.M., Kopell, N.J., 2008. Dynamic cross-frequency couplings of local field potential oscillations in rat striatum and hippocampus during performance of a T-maze task. Proc. Natl. Acad. Sci. U.S.A. 105, 20517–20522.

VanRullen, R., Koch, C., 2003. Is perception discrete or continuous? Trends Cogn. Sci. 7, 207–213.

Varela, F., Lachaux, J.P., Rodriguez, E., Martinerie, J., 2001. The brainweb: phase synchronization and large-scale integration. Nat. Rev. Neurosci. 2, 229–239.

Walker, J.J., Terry, J.R., Lightman, S.L., 2010. Origin of ultradian pulsatility in the hypothalamic–pituitary–adrenal axis. Proc. Biol. Sci. 277, 1627–1633.

Wulff, P., Ponomarenko, A.A., Bartos, M., Korotkova, T.M., Fuchs, E.C., Bahner, F., Both, M., Tort, A.B., Kopell, N.J., Wisden, W., Monyer, H., 2009. Hippocampal theta rhythm and its coupling with gamma oscillations require fast inhibition onto parvalbumin-positive interneurons. Proc. Natl. Acad. Sci. U.S.A. 106, 3561–3566.

Young, C.K., Eggermont, J.J., 2009. Coupling of mesoscopic brain oscillations: recent advances in analytical and theoretical perspectives. Prog. Neurobiol. 89, 61–78.

Please cite this article in press as: Onslow, A.C.E., et al., Quantifying phase–amplitude coupling in neuronal network oscillations, Progress in Biophysics and Molecular Biology (2010), doi:10.1016/j.pbiomolbio.2010.09.007